Tissue-specific BMAL1 cistromes reveal that rhythmic transcription is associated with rhythmic enhancer-enhancer interactions

Joshua R Beytebiere, Alexandra J Trott, Ben Greenwell, Collin A Osborne, Helene Vitet, Jessica Spence, Seung-Hee Yoo, Zheng Chen, Joseph S Takahashi, Noushin Ghaffari, Jerome S Menet[#]

[#] Contact information: menet@bio.tamu.edu

Supplementary Tables

Table S1: genomic location of all 9066 BMAL1 peaks and their target genes
Table S2: motif analysis at BMAL1 peaks (group 5, 6, 7, and group 1 separately).
Table S3: motif analysis at footprints. Table S3A: BMAL1 peak center +/- 100bp (group 5, 6, 7).
Table S3B: motif analysis at footprints within BMAL1 DHS (group 5, 6, 7)
Table S4: ChIA-PET analysis and all annotated PETs with reads on the same chromosome.
Table S5: genomic location of all 67,443 DHS peaks in the mouse liver used for the analysis of DHS interactions.

Supplementary Figures (pages 12-21)
Supplemental Fig. S1-S7

Supplementary Materials and Methods

Animals

Male C57BL/6J and *Bmal1-/-* mice were housed under 12-h light:12-h dark (LD12:12) with food and water available *ad libitum*. *Bmal1-/-* were kindly provided by Christopher Bradfield (Bunger et al. 2000). The age of animals collected was between three and six months old. All experiments were approved by the TAMU Institutional Animal Care and Use Committee (AUP# 2016-0199 and AUP 2013-0158).

BMAL1 chromatin immunoprecipitation

Mice were euthanized by isoflurane anesthesia followed by decapitation, and livers, kidneys, and hearts were collected, rinsed in ice-cold 1X PBS, minced, and immediately homogenized in

1X PBS containing 1% formaldehyde for 10 minutes at room temperature (4ml for livers, 2ml for kidneys, and 1ml for heart). Formaldehyde cross-linking was quenched by adding 2M glycine to a final concentration of 140 mM. Samples were then kept on ice for ten minutes, washed twice with hypotonic buffer (10mM Hepes pH 7.6, 15mM KCl, 0.15% NP-40, 1mM DTT, and 1mM PMSF), and centrifuged at 1500g for 2 minutes at 4ºC. Nuclei were purified by centrifuging on a sucrose cushion (10mM Hepes pH7.6, 15mM KCl, 0.15% NP-40, 24% sucrose, 1mM DTT, 1mM PMSF) at 20,000g for 10 minutes at 4°C, and then washed with hypotonic buffer four times. Sonication for the liver and kidneys were done by resuspending the samples in 12ml per liver and 4.5 ml per kidney of sonication buffer (10mM Tris pH 7.5, 150mM NaCl, 2mM EDTA, 0.25% SDS, 0.2% Triton). Sonication of the heart was done by resuspending the heart in 500 µl of sonication solution (10mM Tris pH 7.5, 150mM NaCl, 2mM EDTA, 0.5% Sarkosyl, 1X protease inhibitor cocktail). Samples were sonicated in 500 µl aliquots to obtain chromatin fragments of about 100-600 bp in length. After sonication, samples were centrifuged at 15,000g for 10 minutes at 4°C, supernatants were moved to a new tube, and inputs (25 µl) and ChIP (200 µl) samples were made. The 200 µl ChIP aliquots were diluted (final concentration: 10mM Tris-Cl pH 7.5, 150mM NaCl, 1% Triton X-100, 0.1% sodium deoxycholate, 0.1% SDS or sarkosyl, 2mM EDTA), 1 µl of BMAL1 antibody (chicken anti-BMAL1) was added and left to rotate overnight at 4ºC. Dynabeads antibody coupling kit (#14311D, Invitrogen) was used with rabbit anti-chicken IgY antibody (# 31104, Invitrogen) to immunoprecipitate BMAL1 chromatin complexes. Dynabeads were washed with IP buffer twice (10mM Tris-Cl pH 7.5, 150mM NaCl, 1% Triton X-100, 0.1% sodium deoxycholate, 0.1% SDS or sarkosyl, 2mM EDTA), resuspended in blocking solution (IP buffer with 1 mg/ml bovine serum albumin and 0.1 mg/ml yeast tRNA) and left rotating overnight at 4°C. After overnight incubation, dynabeads were washed once with final IP buffer, the chromatin was added, and left rotating at 4°C for two hours. BMAL1 immunoprecipitated chromatin was then washed twice with TSEI buffer (10mM Tris pH 7.5, 0.1%SDS, 1% Triton X-100, 2mM EDTA, 150mM NaCl, 1mM DTT, 1X Protease Inhibitor Cocktail), twice with TSEII buffer (10mM Tris pH 7.5, 0.1%SDS, 1% Triton X-100, 2mM EDTA, 500mM NaCl, 1mM DTT, 1mM PMSF), twice with LiCl Buffer III (10mM Tris pH 7.5, 0.25M LiCl, 1% NP-40, 1% Na Deoxycholate, 1mM EDTA, 1mM DTT, 1mM PMSF), twice with TENT buffer (10mM Tris pH 7.5, 1mM EDTA, 150NaCl, 0.1% Triton X-100), and once with TET buffer (10mM Tris pH 7.5, 1mM EDTA, 0.1% Triton). ChIP samples were then resuspended in 200uL of ChIP Elution Buffer (50mM Tris-HCl pH8, 10mM EDTA, 1% SDS, 1mMDTT) while input samples were supplemented with 175 µl of ChIP Elution buffer, and incubated for 6-18 hours at 65ºC.

After the incubation, samples were purified using Qiagen PCR purification columns (# 28106), and efficiency of BMAL1 ChIP was verified by qPCR as described below.

Generation of BMAL1 ChIP-seq libraries and sequencing

BMAL1 and input ChIP-Seq libraries were generated from liver, kidney, and heart samples (n = 3 mice per tissue) using NEBNext® ChIP-Seq Library Prep Master Mix Set (# E6240, NEB) as per the manufacturer's instructions. DNA from ChIP and input were quantified using a Quantus Fluorometer (# E6150, Promega), and 10 ng was used to generate the libraries. DNA end repair was performed with NEBNext End Repair Reaction Buffer and Enzyme Mix for 30 minutes at 20°C. dA-Tailing of end-repaired DNA was performed with NEBNext dA-Tailing Reaction Buffer and Klenow Fragment (3'→5' exo) for 30 minutes at 37°C. Adapter ligation of dA-tailed DNA was performed with Quick Ligation Reaction Buffer, NEBNext Adaptor (1.5 µM), and Quick T4 DNA Ligase. Libraries were generated by PCR amplification of adaptor ligated DNA using NEBNext Multiplex oligonucleotides and Phusion Taq (M0530S). Libraries were amplified for 16 cycles. Libraries were quantified with qPCR with TRUseq library standards, and with a Quantus Fluorometer. DNA cleanup between each reaction was performed using Solid Phase Reversible Immobilization (SPRI) beads generated in the lab from Sera-mag SpeedBeads (# catalog number 09-981-123, Thermo-Fisher). BMAL1 ChIP-seq and input libraries were sequenced using an Illumina NextSeq with a sequence length of 76 bp.

BMAL1 ChIP-qPCR

Chromatin Immunoprecipitation was performed as described above with the following exceptions. After tissue collection, tissues were flash frozen in liquid nitrogen and kept at -80ºC. Nuclei extraction was conducted using seven samples at a time (6 time points in wild-type mice -ZT2, ZT6, ZT10, ZT14, ZT18, and ZT22-, and the ZT6 sample from *Bmal1-/-* mouse) to minimize inter-individual variations, and nuclei were flash-frozen in glycerol storage buffer (10mM Tris-Cl pH 7.5, 50mM NaCl, 2mM EDTA, 50% glycerol, 1mMDTT, 0.15mM spermine, 0.5mM spermidine, 1X PIC). BMAL1 ChIPs were also performed using seven samples at a time as described above, except for the BMAL1 antibody (# ab3350, abcam) and the Dynabeads protein G (# 10004D, Invitrogen).

qPCR was performed using the BIO-RAD iTaq Universal SYBR Green Supermix (# 1725124, and BIO-RAD CFX Connect). ChIP fold enrichment was calculated as the ratio between *Dbp* 1st intron ChIP signal normalized to input and intergenic region ChIP signal normalized to input. The primer sequences used are:

Dbp 1st intron (forward): ATGCTCACACGGTGCAGACA
Dbp 1st intron (reverse): CTGCTCAGGCACATTCCTCAT
Intergenic region (forward): CTTTTAATGAGGCTGTGTGGA
Intergenic region (reverse): ACTCCCTTGCGAATGTCCTA

Sequencing datasets and alignment to the mouse genome

All public datasets were downloaded from NCBI or https://encodeproject.org (unless noted below) as fastq or Short Read Archive (SRA) file formats. To avoid issues due to the utilization of different protocols/procedures for each tissue, each of the liver, kidney and heart ChIP-Seq, DNase-Seq and mRNA expression datasets used in cross-comparisons were generated for the from the same research laboratory. Accession number are as follow:

(i) H3K27ac ChIP-seq (comparison between tissues): downloaded from https://encodeproject.org, accession numbers GSM1000093 (heart), GSM1000140 (liver), and GSM1000092(kidney).

(ii) H3K4me1 ChIP-seq: downloaded from https://encodeproject.org, accession numbers GSM769025 (heart), GSM769023 (kidney), and GSM769015 (liver).

(iii) DNase-seq: downloaded from https://encodeproject.org, accession numbers GSM1014166 (heart), GSM1014193 (kidney) and GSM1014195 (liver).

(iv) RNA-seq and microarray datasets: downloaded from the NCBI website, accession numbers GSE54652 (Zhang et al. 2014).

Some other datasets were also use to further characterize tissue-specific BMAL1 DNA binding:

(v) Mouse liver H3K27ac and RNA Polymerase II ChIP-seq (time-course in wild-type and *Bmal1*$^{-/-}$ mice): downloaded from the NCBI website, accession number GSE60430 (Sobel et al. 2017).

(vi) Mouse liver DNase-Seq datasets from wild-type and *Bmal1*$^{-/-}$ mice: downloaded from the NCBI website, accession number GSE60430 (Sobel et al. 2017).

(vii) Mouse liver PER1, PER2, CRY1, and CRY2 ChIP-Seq datasets: downloaded from the NCBI website, accession number GSE39977 (Koike et al. 2012).

(viii) Mouse liver CREB ChIP-Seq datasets: downloaded from the NCBI website, accession number GSE45674 (Everett et al. 2013).

(ix) Mouse liver MYC and TEAD4 ChIP-Seq datasets: downloaded from the NCBI website, accession number GSE83869 (Croci et al. 2017).

(x) Mouse liver CTCF, GABPA, CBP, p300, HNF4A, CEBPA, HNF1A, and HNF6 ChIP-Seq datasets: downloaded at https://www.ebi.ac.uk/arrayexpress/experiments/E-MTAB-941/ (Faure et al. 2012).

(xi) Mouse liver BCL6 and STAT5 ChIP-Seq datasets: downloaded from the NCBI website, accession number GSE31578 (Zhang et al. 2012b).

(xii) Mouse liver ERα ChIP-Seq datasets: downloaded from the NCBI website, accession number GSE52351 (Gordon et al. 2014).

(xiii) Mouse liver REV-ERBα ChIP-Seq datasets: downloaded from the NCBI website, accession number GSE34020 (Cho et al. 2012).

(xiv) Mouse liver GR ChIP-Seq datasets: downloaded from the NCBI website, accession number GSE59752 (Lim et al. 2015).

(xv) Mouse liver PPARα, LXR, and RXRα ChIP-Seq datasets: downloaded from the NCBI website, accession number GSE35262 (Boergesen et al. 2012).

(xvi) Mouse liver FOXA1 and FOXA2 ChIP-Seq datasets: downloaded from the NCBI website, accession number GSE17067 (MacIsaac et al. 2010).

SRA files were converted to fastq files using SRA toolkit (Leinonen et al. 2011). ChIP-seq and DNase-seq datasets were aligned to the mouse genome (version mm10) using bowtie2 (Langmead and Salzberg 2012) using the parameters: -x and --end-to-end. Uniquely mapped reads were only considered for analysis, and up to 3 duplicated sequences were kept for each BMAL1 ChIP-Seq dataset. The heart BMAL1 ChIP-Seq replicate 1 dataset contains two technical replicates that were merged into a single bam file, which was then randomly downsampled using samtools from 47,936,219 read to 17,253,305 reads to avoid overrepresentation of one replicate in the final merged file comprising the three biological replicates. All bam files from the heart were then merged for a total read count of 36,975,623 reads (replicate 1: 17,253,305 reads; replicate 2: 11,994,180 reads; replicate 3: 7,728,138 reads). The kidney biological replicate 1 was also downsampled using samtools from 26,840,611 reads to 8,856,833 reads. All bam files from the kidney were then merged for a total of 26, 930,789 reads (replicate 1: 8,856,833 reads; replicate 2: 7,381,236 reads; replicate 3: 10,692,720 reads). None of the liver samples were downsampled, and the bam files were merged using samtools for a total of 34,846,537 reads (replicate 1: 10,966,215 reads; replicate 2: 11,265,139 reads; replicate 3: 12,615,183 reads). Visualization files were generated using bedtools (Quinlan and Hall 2010) and normalized to 10,000,000 reads. Input files were processed individually and then merged as bam files using samtools.

For DNase-seq datasets, bam files from all technical and biological replicates were merged and no downsampling was performed. Reads from the RNA-Seq dataset were trimmed using fastx_trimmer (http://hannonlab.cshl.edu/fastx_toolkit/) with the following parameters -f 1 -l 100 -Q 33, and aligned to the genome using STAR (Dobin et al. 2013) with the default parameters and the option: --outFilterIntronMotifs RemoveNoncanonical. Gene expression data were retrieved using cufflinks (Trapnell et al. 2012) and the genome version GRCm38.p5_M14 and default parameters.

Sequencing datasets analysis

BMAL1 ChIP-seq and DNase-seq peak calling. Peak calling for both BMAL1 ChIP-seq and DNase-seq data was performed with findPeaks from the HOMER suite (Heinz et al. 2010). A minimum local enrichment of 4-fold was set up as necessary, and the following parameters were used: -style factor and -i (for BMAL1 ChIP-Seq) or -style dnase and -region (for DNase-Seq). No input was used to identify DNase-seq peaks. Overlap between ChIP-Seq or DNase-Seq peaks was determined using the function intersectBed from Bedtools suite (Quinlan and Hall 2010) using default parameters. Heatmaps were generated using the Rscript pheatmap.R.

Assignment of BMAL1 peaks to their target genes. BMAL1 peaks were assigned to their target genes using the perl script annotatePeaks.pl from the HOMER suite with the mm10 mouse genome as a reference (Heinz et al. 2010). The HOMER gene annotation script outputs each peak into the following categories: (i) Promoter-TSS, corresponding to TSS - 10kb to TSS + 1kb, (ii) Transcription termination site (TTS), corresponding to TTS - 100 bp to TTS + 1kb, (iii) exons, (iv) introns, and (v) intergenic, which corresponds to peaks located upstream of the TSS by more than 10 kb and downstream the TTS by more than 1 kb. Intron and exon assignments were not adjusted from the output of HOMER annotatepeaks.pl. BMAL1 peaks labeled as intergenic were not assigned to a target gene.

Quantification of ChIP-Seq and DNase-Seq signal at BMAL1 ChIP-Seq peaks. ChIP-seq and DNase-seq signal was calculated using scripts from Bedtools (Quinlan and Hall 2010), the uniquely mapped reads (mm10 version) and the genomic coordinates of BMAL1 ChIP-seq peaks (Table S1) or mouse liver DHS peaks (Table S5). Signal was calculated in a ± 250 bp region from the peak center for DNase-seq as well as for BMAL1 and other TF ChIP-seq signal, and in a ± 1 kb region from the peak center for H3K27ac ChIP-Seq signal.

Footprint detection. Detection of footprints was performed using the python script wellington_footprints.py from the pyDNase suite (Piper et al. 2013; Piper et al. 2015). All parameters were set to default, and a p-value of -20 was used along with an FDR of 0.01. Wig files generated by wellington_footprints.py were converted to BigWig files with the wigToBigWig algorithm downloaded at https://genome.ucsc.edu/.

Motif analysis at BMAL1 peaks and footprints at BMAL1 peaks and enhancers. Motif analysis was performed at BMAL1 DNA binding sites (genomic location of BMAL1 ChIP-Seq peaks) using the perl script findMotifsGenome.pl from the HOMER suite (Heinz et al. 2010), using the parameter -size 200. Motifs were considered as significantly enriched if the q-value was less than 0.05. Motif enrichment was calculated based on the background from the output of findMotifsGenome.pl. Motif analysis at footprints located with BMAL1 peaks and BMAL1 DNase I hypersensitive sites (peak center ± 15bp) has been performed similarly.

Quantification of DNase I cuts at E-boxes and other TF binding motifs. The genomic location of DNase I cuts was retrieved from DNase-Seq datasets by reporting the position and strandness of the first nucleotide of each read in a bam file. Average DNase I cut signal was calculated at E-boxes and other TF binding motifs using scripts from Bedtools (Quinlan and Hall 2010). Quantification of the average DNase I cut signal at control peaks (*i.e.*, TF ChIP-Seq peaks that do not exhibit BMAL1 ChIP-Seq signal; Fig. 3I) was performed by randomly selecting an equivalent number of TF ChIP-Seq peaks without BMAL1 to the number of peaks with BMAL1. Because most TF ChIP-Seq peaks with BMAL1 signal exhibit strong DNase-Seq signal (*i.e.*, most of them are within the strongest DHSs), the random selection was performed by matching the number of peaks within each DNase-Seq signal decile. This process was repeated 1,000 times, and the average of 1,000 iterations calculated.

Detection of E-box and dual E-box motifs. Generation of motifs for E-boxes and dual E-boxes was performed with the perl script seq2profile.pl from the HOMER suite (Heinz et al. 2010). The E-boxes considered for analysis were as follows CACGTG, CACGNG and CACGTT. These E-boxes contained only one mismatch from the canonical motif and were found to be functional CLOCK-binding motifs *in vitro* (Yoshitane et al. 2014). The dual E-box motif tolerates up to two mismatches between the two E-boxes and contains a spacer of either six or seven base pair.

Gene ontology analysis. Gene ontology was performed using the perl script annotatePeaks.pl from the HOMER suite (Heinz et al. 2010), with the parameter -go and mm10 genome. HOMER assigns target genes based on the closest gene to the BMAL1 binding region, and then searches for enriched functional categories.

Rhythmic expression analysis. Rhythmic expression of BMAL1 target genes was determined using public microarray datasets performed in the same research lab (Zhang et al. 2014). Files containing expression values for each microarray probe were downloaded from the NCBI website (GSE54652), and no analysis of the original files were performed. Rhythmic gene expression was determined using JTK cycle (Hughes et al. 2010) with the following parameters: timepoints 18-64, and all other parameters were left to default, and was considered significant if q-value < 0.05. The output regarding phase of expression, which is reported for every gene, was used in the ChIA-PET analysis. For results presented in Fig. 5A and 5B, genes targeted by two or more BMAL1 ChIP-Seq peaks assigned to different categories (*e.g.*, a gene targeted by two BMAL1 peaks: one common to all three tissues, and one specific to the liver) were not considered.

Data from GTEX portal. Graphs in Supplemental Fig. S3C displaying the RPKM values of different TFs in human liver, kidney, and heart (atrial appendage and left ventricle) were retrieved from GTEX portal (Consortium 2013) in April 2016.

Mouse liver Pol II ChIA-PET

Pol II ChIA-PET experiments were performed using mouse livers collected at either ZT6 or ZT18, with three biological replicates per time point and following previously published protocols (Fullwood and Ruan 2009; Li et al. 2010; Zhang et al. 2012a). Pol II ChIP, which is the starting point of the ChIA-PET experiment (Fig. 6A), was performed similarly to BMAL1 ChIP with the following modifications:

(i) Livers were collected, rinsed in ice-cold 1X PBS, flash frozen in liquid nitrogen, and stored at -80°C. Frozen livers were crushed to a fine powder in liquid nitrogen using a mortar, and resuspended in 1X PBS containing the crosslinking reagents. One ChIA-PET experiment (JM11) was performed on livers crosslinked with 1% formaldehyde for 10 minutes at room temperature (single crosslinking), and two experiments (JM08 and JM12) were performed on livers first crosslinked with 1.5 mM EGS for 20 minutes at room temperature, and then for 10 additional minutes with 1% formaldehyde (dual crosslinking).

(ii) Nuclei were sonicated in 10 mM Tris pH 7.5, 150 mM NaCl, 2 mM EDTA, 0.5% SDS, 0.2% Triton, 1X protease inhibitor cocktail. Because large amounts of starting material were required, sonicated liver chromatin from 3-7 mice were pulled together, resulting in chromatin amounts ranging from 1.3 mg to 4.1 mg in a volume of ~10 ml. Chromatin samples were diluted 5-fold to obtain a final concentration of ChIP buffer of 10mM Tris-Cl pH 7.5, 150mM NaCl, 1% Triton X-100, 0.1% sodium deoxycholate, 0.1% SDS, 1X protease inhibitor cocktail. Pol II ChIP were performed in 50 ml canonical tube with 65 µg of anti-RNA Polymerase II 8WG16 monoclonal antibody (# MMS-126R, Covance). Immunoprecipitated chromatin was washed once with TSEI buffer, once with TSEII buffer, once with LiCl Buffer III, and once with TET buffer (see above for buffer composition). Beads were finally resuspended in 2 ml of 1X TE buffer supplemented with 1X protease inhibitor cocktail.

(iii) A sample corresponding to 1/40th of each ChIP was set apart and processed for DNA purification and assessment of ChIP enrichment by qPCR. Enrichment was calculated as the ratio between *Aldob* TSS ChIP signal normalized to input and intergenic region ChIP signal normalized to input. The *Aldob* primer sequences used are (forward) TGTTATCATTAACCCAGCTTGC and (reverse) CTGCCACCTCACACAGCTT. The intergenic region primer sequences are described above.

Libraries were generated following published protocols (Fullwood and Ruan 2009; Li et al. 2010; Zhang et al. 2012a). Immunoprecipitated chromatin was end-repaired, processed for ligation with biotinylated half-linkers, and 5' phosphorylated while still complexed with Pol II antibodies on magnetic beads. Chromatin was then eluted, diluted to a final volume of 10 ml, and used for the proximity ligation step (performed for a minimum of 16 hours at 4ºC under extremely diluted conditions, i.e., < 0.2 ng DNA/µL, to favor ligation events within individual crosslinked chromatin complexes). Following the proximity ligation step, chromatin was treated with proteinase K, reverse crosslinked, and the DNA purified. ChIA-PET DNA was then digested with MmeI, immobilized on streptavidin beads, and ligated to the ChIA-PET adapters. The DNA samples were finally proceeded through nick translation and a PCR amplification step to generate the library (number of cycles indicated in Supplemental Fig. S7A). Libraries were ran on an agarose gel, and fragment of ~229 bp were gel-extracted, purified, and quantified using a quantus fluorometer.

Sequencing and computational analysis of Pol II ChIA-PET libraries

Sequencing and read alignment to the mouse genome. ChIA-PET libraries were sequenced on a HiSeq 2000 (JM08 and JM12) or a MiSeq (JM11) to a length of 90 bp (JM08), 100 bp (JM11), and 125 bp (JM12). Reads from the fastq files were processed to extract the tag 1 and 2 (i.e., read 1 and 2) along with their accompanying half-linker code using a custom-made Python script and generate two fastq files (R1 and R2 file) containing the sequence identifier, the raw sequence, and the sequence quality values for each tag. These two files were then aligned to the mouse genome (mm10 version) as paired-end reads using bowtie2 and the options -X 5 and --fast.

Paired-End Tags (PETs) filtering. Only paired tags with both reads mapping uniquely to the mouse genome were considered in our analysis. First, PETs were parsed based on the half-linker barcodes into non-chimeric PETs (specific products) or chimeric PETs (non-specific products) (Fig. 6A). Then, duplicated PETs (i.e., PCR duplicates) were removed for both chimeric and non-chimeric products. PETs with a tag location shifted by 1 bp compared to an existing PET were also considered as PCR duplicates and removed. Identical PET found at both ZT6 and ZT18 for the same experiment (JM08, JM11 or JM12), and which likely originate from PCR errors due to priming from half-linkers, were also filtered out. Quality of the ChIA-PET experiments was assessed by determining the percentage of non-chimeric/specific *vs.* chimeric/non-specific PETs (Supplemental Fig. S7C), the proportion of PETs with both tags being on the same chromosome (Supplemental Fig. S7D), and the distance between each tag (Supplemental Fig. S7B, D).

Functional analysis of the mouse liver Paired-End Tags (PETs). PETs with both reads on the same chromosome and with a distance between reads ≥ 500 bp were only considered in our analysis (n = 218,639 PETs, Table S4). For all PETs, each of the two tags was extended to 200 bp (tag location ± 100 bp) and this tag genomic location (chr:start-end) was used to map tags to (i) a gene, and (ii) a DNase I hypersensitive site, using intersectBed from bedtools (Quinlan and Hall 2010). Gene coordinates were defined at TSS - 10kb to TTS + 1kb. Mapping to DHS was performed using a more stringent analysis of the mouse liver DNase-Seq datasets from ENCODE (Table S5), and which mostly reports stronger DHSs (see Fig. 6D). This is because relaxation of the parameters for DNase-Seq analysis often consolidate several distinct DHS peaks into one DHS of several kilobases, thereby resulting into reporting PETs into the same DHS when both reads were distinctively located into two different DHS peaks. DHSs harboring a mouse liver BMAL1 peak were identified with intersectBed between the DHS peak list

described above and the list of mouse liver ChIP-Seq peaks generated in this manuscript (Table S1). To validate that mouse liver PETs contribute to gene transcription (Fig. 6B, 6C), we used public mouse liver Nascent-Seq datasets (Menet et al. 2012), and averaged values for each of the 12 independent samples. Finally, we considered genes to be rhythmically expressed based on the analysis of the microarray datasets from Zhang and collaborators (Zhang et al. 2014), as described above.

Statistical analysis

Statistical analysis was carried out in JMP®, Version 12.0.1 SAS Institute., Cary, NC, 1989-2007. ChIP-Seq and DNase-Seq signals were analyzed using a Kruskal-Wallis test, and post-hoc analysis with a Wilcoxon each pair test. Analysis of TF mRNA expression between the three tissues was performed using a one-way ANOVA. Analysis of the differences in BMAL1 peaks genomic locations was performed using a chi-square test, and differences in the number of BMAL1 peaks per genomic locations we analyzed by a Fisher's exact test. Spearman correlation was used to determine the degree of correlation between signals (e.g., ChIP-Seq with DNA-Seq) or signal between tissues. Results were considered significant if p-value < 0.05 for the Kruskal-Wallis, student t-test and ANOVA tests, and p-value < 0.01 for Fisher's exact test.

Data availability

The sequencing datasets generated in this paper (BMAL1 ChIP-seq and Pol II ChIA-PET) have been deposited to GEO under the accession code GSE110604.

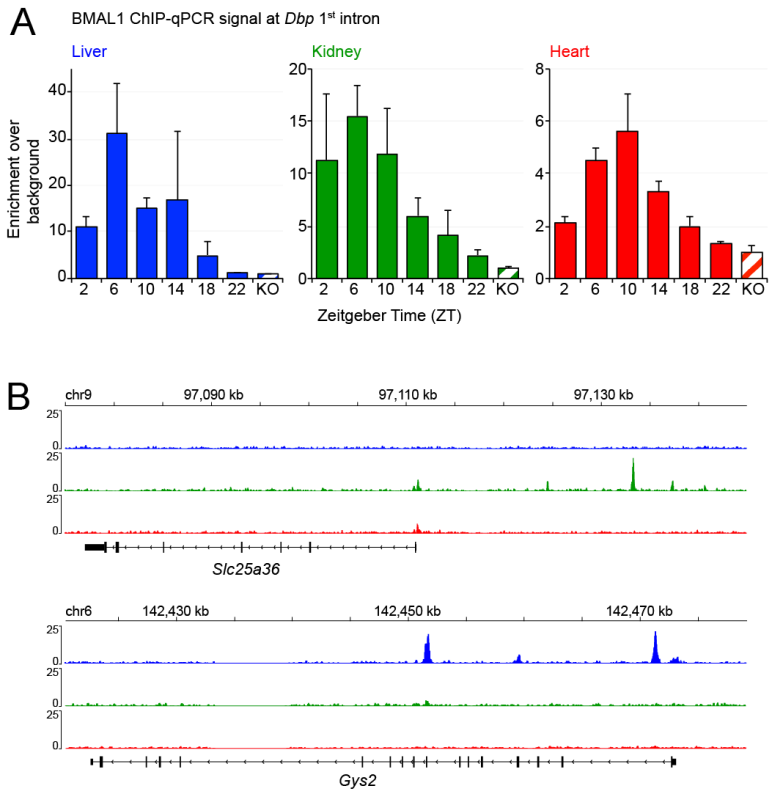

Supplemental Figure 1. BMAL1 cistromes are largely tissue specific. (related to Fig. 1) **(A)** BMAL1 ChIP-qPCR signal at *Dbp* 1st intron over the course of the day in the mouse liver (blue), kidney (green), and heart (red). Tissues were collected in wild-type mice at ZT2, ZT6, ZT10, ZT14, ZT18, and ZT22, and in *Bmal1* knockout mice at ZT6 for negative control. ChIP-qPCR signal normalized to the input signal corresponds to the average ± s.e.m. of 3 biological replicates, and the ratio ChIP/input was set to 1 for the *Bmal1* knockout mice samples. **(B)** Genome browser view of BMAL1 ChIP-Seq signal in the liver (blue), kidney (green), and heart (red) at *Slc35a6* and *Gys2* gene loci. BMAL1 ChIP-Seq signal is tissue-specific, with kidney-specific BMAL1 binding at *Slc35a6*, and liver-specific BMAL1 signal at *Gys2*.

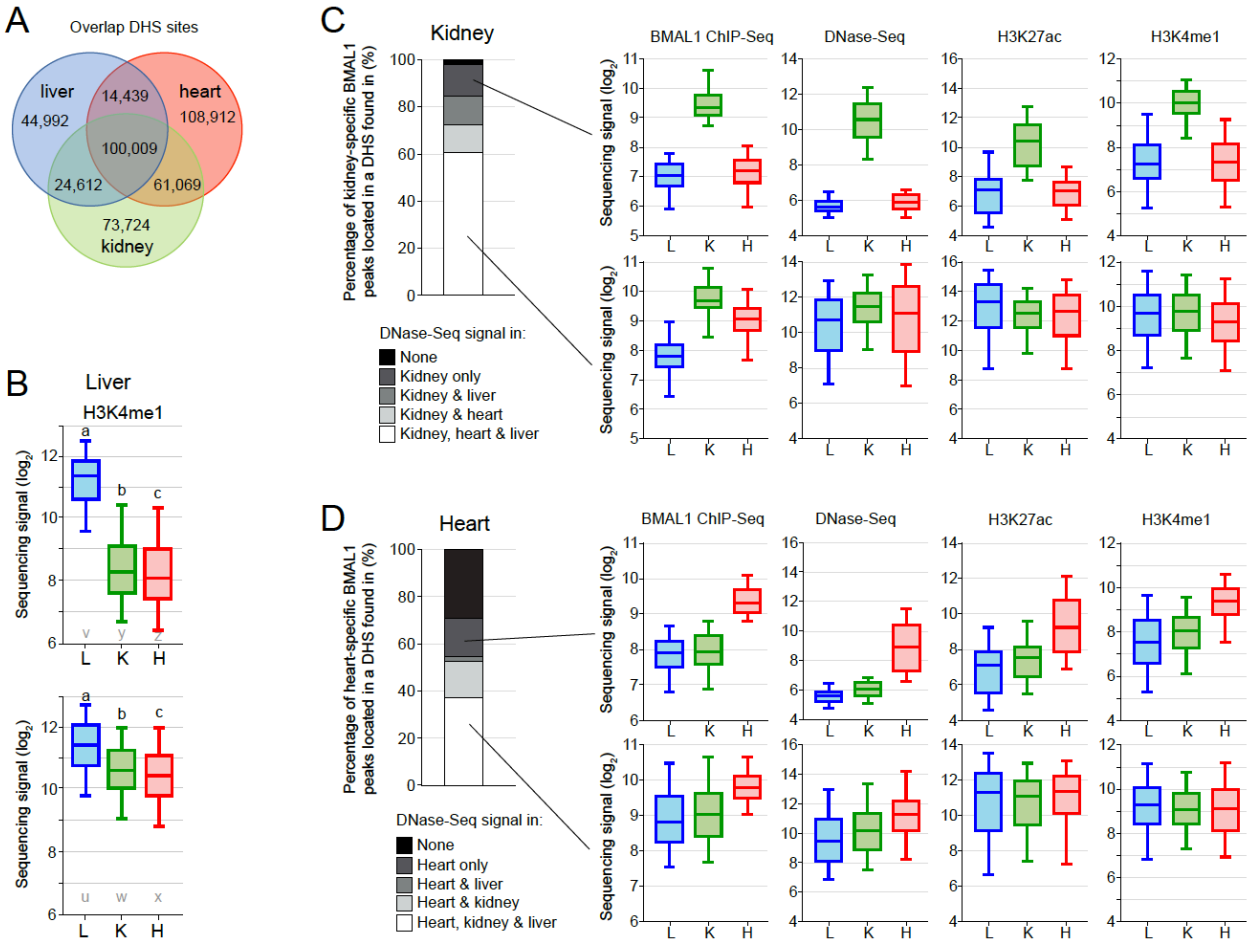

Supplemental Figure 2. The chromatin environment shapes tissue specific BMAL1 binding. (related to Fig. 2)
(A) Venn diagram depicting the overlap of DNase hypersensitive sites (DHSs) between the mouse liver, kidney, and heart. DNase-Seq datasets were downloaded from the ENCODE project, and analyzed to define DHSs in each of the three tissues. Of the total 427,748 DHSs among the mouse liver, kidney, and heart, 100,009 are common to all three tissues. **(B)** H3K4me1 ChIP-seq signal (log2 scale) in the mouse liver, kidney, and heart at liver-specific BMAL1 peaks located in liver-specific DHSs (top), or at liver-specific BMAL1 peaks located at DHSs common to the liver, kidney and heart. H3K4me1 ChIP-Seq datasets were downloaded from the ENCODE project, and signal was calculated at BMAL1 peak center ± 1kb. **(C)** Left: Stacked bar chart representation of the percentage of kidney-specific BMAL1 peaks located within kidney-specific DHSs or DHSs found in other tissues. Right: Boxplot representation of BMAL1 ChIP-seq, DNase-seq, H3K27ac ChIP-seq and H3K4me1 ChIP-seq signals at kidney-specific BMAL1 peaks located at a kidney-specific DHSs or at a DHSs common to the liver, kidney and heart. Signal for BMAL1 ChIP-seq and DNase-seq was calculated at BMAL1 peak center ± 250 bp, and at BMAL1 peak center ± 500 bp for ChIP-seq of histone modifications. **(D)** Similar to panel C, but for heart-specific BMAL1 peaks.

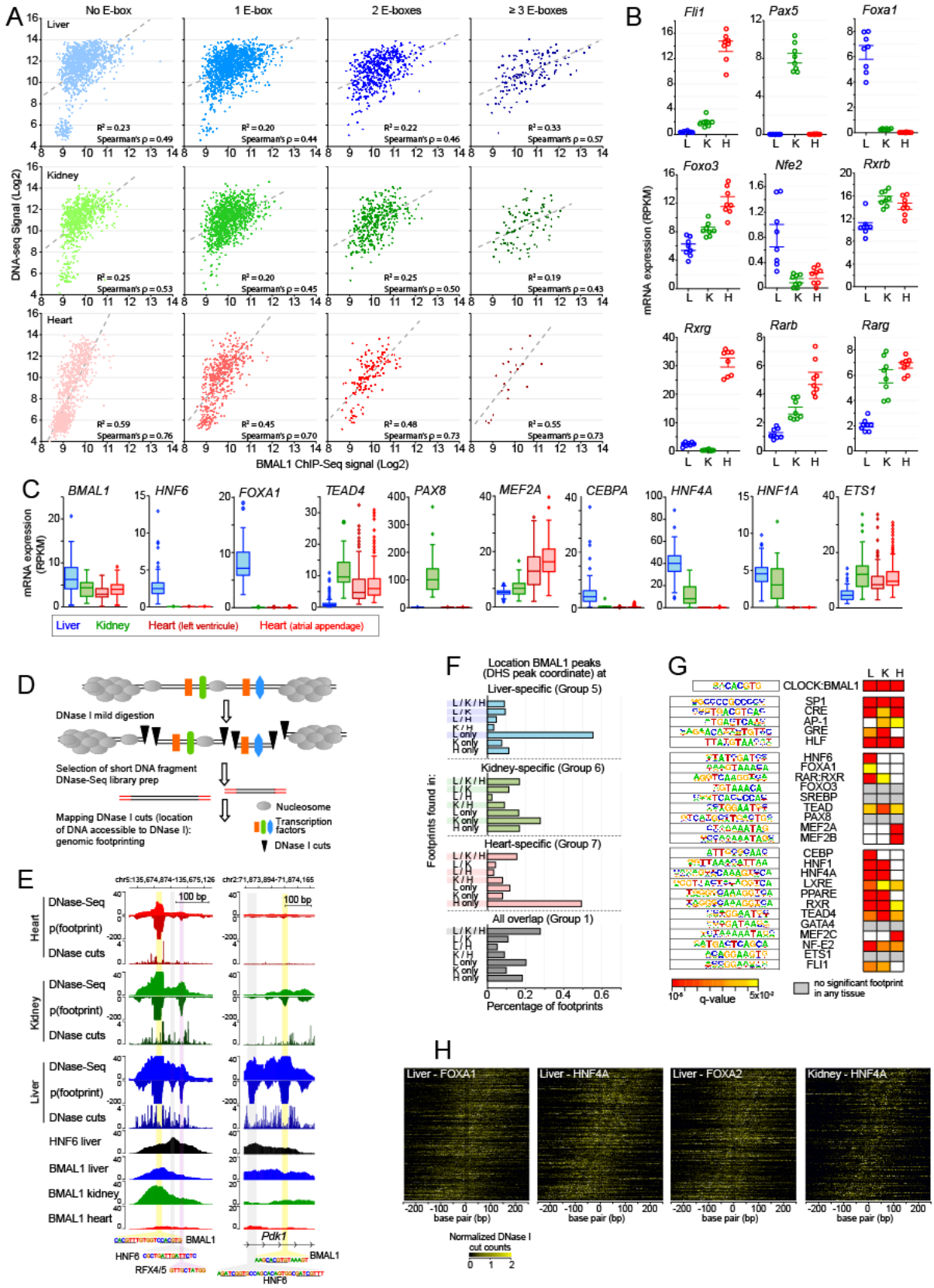

Supplemental Figure 3. Tissue-specific transcription factors may contribute to tissue-

specific BMAL1 DNA binding. (related to Fig. 3)
(A) Correlation between DNase-seq signal and BMAL1 ChIP-seq signal for liver- (blue), kidney- (green) and heart- (red) specific BMAL1 peaks parsed based on the number of E-boxes. The E-boxes used in the analysis were CACGTG, CACGNG, and CACGTT. BMAL1 ChIP-seq signal and DNase-seq signal, which are represented in log2 scale, were calculated at BMAL1 peak center ± 250 bp. **(B)** mRNA expression in the mouse liver, kidney, and heart of *Bmal1* and transcription factors whose motifs were enriched at BMAL1 ChIP-Seq peaks. mRNA expression was calculated using public RNA-Seq datasets (Zhang et al. 2014) from samples collected over the course of the 24-hr day. **(C)** mRNA expression (RPKM) in human liver (blue), kidney (green), and heart (red, left ventricle and atrial appendage) for the tissue-specific transcription factors displayed in Fig. 3C, D, and E. Data were retrieved from the GTEx portal (https://www.gtexportal.org/home/) (Consortium 2013). **(D)** Illustration of the DNase-Seq protocol, and the analysis of DNase I cuts that reveal footprints at DNase I hypersensitive sites (DHSs). Mild DNase I digestion of nuclei preserves closed chromatin and transcription factors/nucleosomes-bound regions from DNase I cutting. Thus, mapping regions uncut by DNase I at DHSs can reveal regions that are occupied by transcription factors and/or nucleosomes. **(E)** Genome browser view of DNase-seq signal, footprints p-value, DNase I cut sites, and BMAL1 ChIP-seq signal in the mouse liver (blue), kidney (green), and heart (red) at two BMAL1 DNA binding sites. DNase-Seq datasets were downloaded from the ENCODE project, and footprint p-value visualization files were generated using pyDNase (Piper et al. 2013; Piper et al. 2015). Mouse liver HNF6 ChIP-Seq signal, which was downloaded from a public dataset (Faure et al. 2012), is also displayed. Both BMAL1 peaks exhibit significant footprints at motifs corresponding to E-boxes, as well as to motifs for other transcription factors including the liver-specific transcription factor HNF6. **(F)** Distribution of DNase I footprints detected at the genomic coordinate of the DHSs bound by BMAL1, and parsed based on the tissue(s) they were found in. Analysis was performed at BMAL1 peaks that are liver-specific (blue), kidney-specific (green), heart-specific (red), or common to all three tissues (grey). **(G)** Motif enrichment of transcription factors performed at the DNase I footprints identified within the genomic coordinate of the DHS bound by BMAL1, for liver-, kidney-, and heart-specific BMAL1 peaks (footprint center ± 15 bp). Enrichments are displayed if q-value < 0.05, and colored in grey in no significant footprint is detected in any of the three tissues. **(G)** Heatmaps representing the DNase I cuts at BMAL1 peaks containing an E-box and a motif for another transcription factor. DNase I cut signal is centered on the E-box and sorted based on the distance between the E-box and the transcription factor motif. Scale corresponds to E-box center ± 250bp.

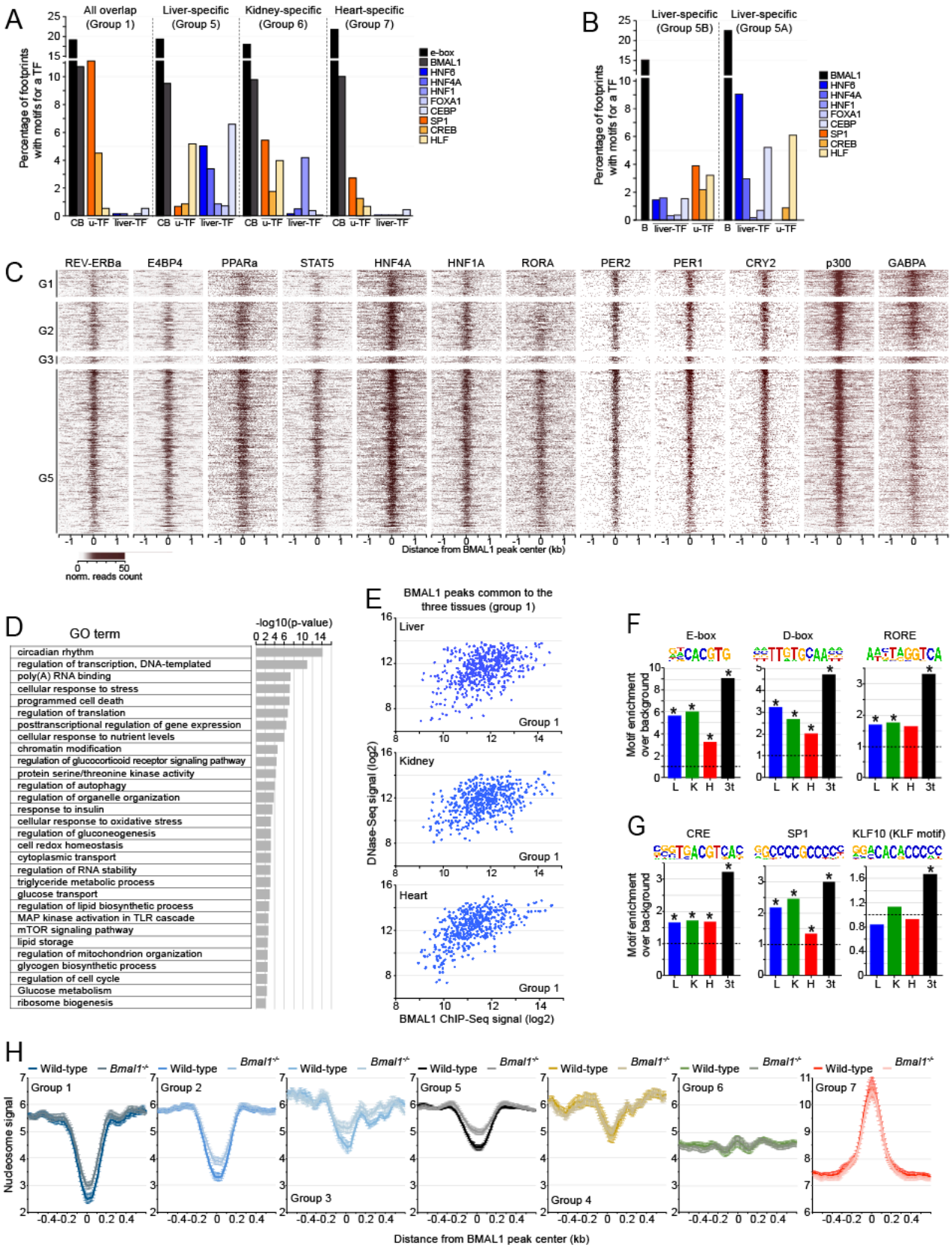

Supplemental Figure 4. Differential binding of transcription factors between tissue-

specific and common BMAL1 peaks. (related to Fig. 4)
(A, B) Percentage of footprints for BMAL1 (black), liver-specific transcription factors (HNF6, HNF4A, HNF1, FOXA1, CEBP; blue), and ubiquitous transcription factors (SP1, CREB, HLF; orange) identified at (E) BMAL1 peaks common to all three tissues (group 1), BMAL1 peaks that are liver-specific (group 5), kidney-specific (group 6), and heart-specific (group 7), or at (F) liver-specific peaks that are located at a liver-specific DHS (group 5A) or located at a DHS that is common to the liver, kidney, and heart. **(C)** Heatmap representation of mouse liver ChIP-Seq signal for different transcription factors at BMAL1 peaks ordered based on BMAL1 ChIP-Seq signal (as in Fig. 1B) for the group 1 (peaks common to all three tissues), 2 (peaks common to the liver and kidney), 3 (peaks common to the liver and heart), and 5 (liver-specific peaks). ChIP-Seq datasets were retrieved from public depositories (see methods for details). **(D)** Gene ontology analysis of the genes targeted by BMAL1 peaks common to all three tissues (p-value < 0.05). **(E)** Correlation between DNase-seq and BMAL1 ChIP-seq signals for BMAL1 peaks that are common to all three tissues. Signal was calculated at BMAL1 peak center ± 250 bp in the mouse liver, kidney, and heart, and is displayed in log2 scale. **(F, G)** Enrichment for the motifs of clock genes (F) and u-TFs (G) at tissue-specific BMAL1 peaks (liver in blue, kidney in green, and heart in red) or BMAL1 peaks common to the three tissues (black). Asterisks illustrate a q-value < 0.05. **(H)** Nucleosome signal at BMAL1 DNA binding sites parsed based on tissues in which BMAL1 peaks were detected (group 1 to 7, see above). Nucleosome signal was retrieved from liver MNase-Seq datasets of wild-type and *Bmal1*$^{-/-}$ mice (Menet et al., 2014), which consists of 6 time points each separated by 4 hours with n = 4 mice for each time point, and is displayed as the average of the 24 datasets ± s.e.m.

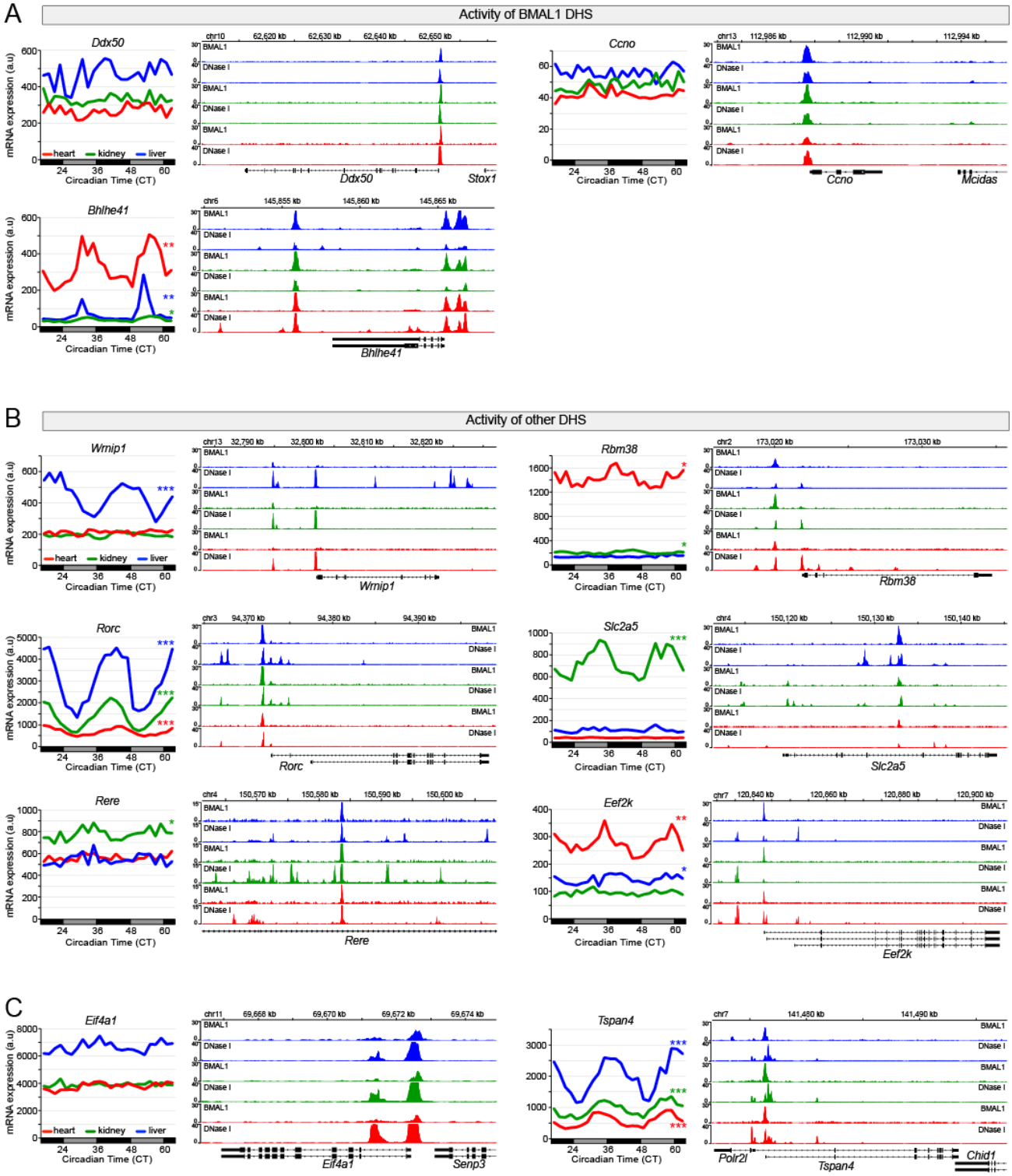

Supplemental Figure 5: Tissue-specificity of rhythmic BMAL1 target gene expression relies on the transcriptional activities of DHS bound by BMAL1, but also other DHS.
(related to Fig. 5)
(A-C) mRNA expression (left) and genome browser view (right) of BMAL1 ChIP-seq and DNase-seq signals in the mouse liver (blue), kidney (green), and heart (red). Rhythmic expression determined by JTK-cycle is defined as *** if q-value < 0.001, ** if q-value < 0.01, and

* if q-value < 0.05. Panel A represents examples for which the activity of BMAL1 DHS likely contributes to the differences in mRNA expression, whereas panels B and C represent examples for which the activity of other DHS likely contributes to BMAL1-mediated rhythmic transcription. The activity of these other enhancers often enhances (rhythmic) target gene expression (B), but it can also lead to decrease (rhythmic) gene expression (C).

A

	Single X-link	Dual X-link (1)	Dual X-link (2)
Nb of Pol II ChIA-PET lib	2	4	2
ChIP starting material per library (ng)	24,311 ± 1,779 (29,827; 21,796)	338 ± 91 (140; 533; 319;361)	304 ± 14 (290; 318)
Nb amplification cyles	14	20	16
Nb reads (total)	17,029,738	341,886,784	340,510,620
Reads passing QC	15,686,931	284,983,965	317,109,401
Nb uniquely mapped reads	2,026,322	44,020,678	45,238,532
Non-chimeric reads	1,498,691	31,339,229	27,954,216
Unique non-chimeric reads (percentage)	1,439,048 (96.02%)	559,254 (1.78%)	851,265 (3.04%)
Chimeric reads	527,631	12,681,449	17,284,316
Unique chimeric reads (%) (percentage)	504,807 (95.67%)	232,707 (1.84%)	562,020 (3.25%)

B

	Single X-link		Dual X-link (1)		Dual X-link (2)	
	Non-chimeric	Chimeric	Non-chimeric	Chimeric	Non-chimeric	Chimeric
Pairs < 3kb (%)	88,790 (6.17%)	1,248 (0.25%)	128,276 (22.9%)	583 (0.25%)	123,326 (14.4%)	3,466 (0.62%)
3kb < pairs < 8kb (%)	871 (0.06%)	21 (0.04%)	1068 (0.20%)	7 (0.003%)	2,462 (0.28%)	141 (0.025%)
8kb < pairs < 200kb (%)	588 (0.04%)	84 (0.016%)	1,140 (0.20%)	34 (0.01%)	2,487 (0.29%)	163 (0.029%)
Pairs > 200kb (%)	72,743 (5.05%)	27,102 (5.39%)	23,229 (4.15%)	12,149 (5.22%)	40,220 (4.72%)	29,872 (5.32%)
Extra-chrom. reads (%)	1,276,056 (88.7%)	467,352 (94.4%)	405,541 (72.5%)	219,776 (94.4%)	683,160 (80.2%)	528,378 (94.0%)

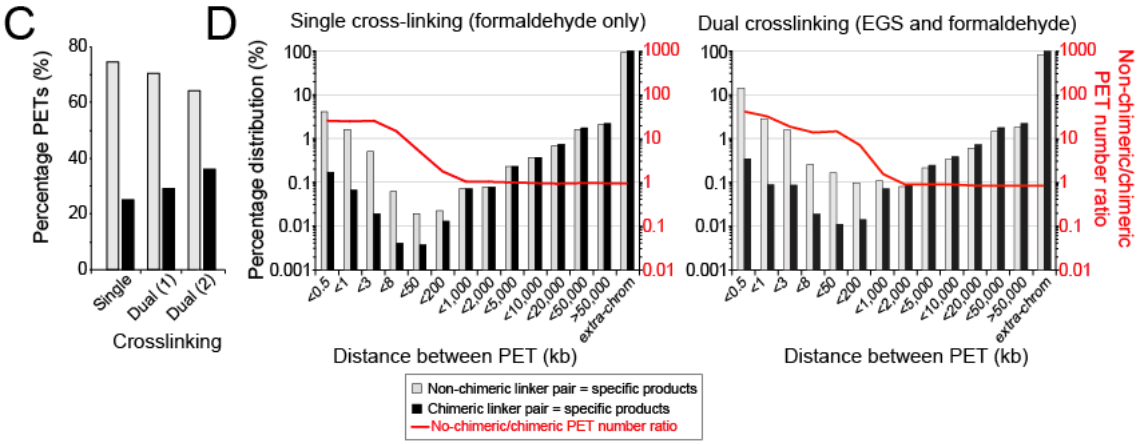

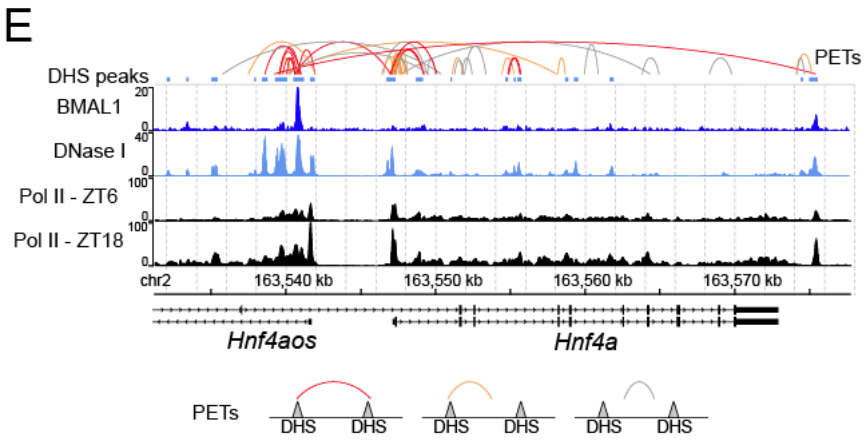

Supplemental figure 6: Pol II ChIA-PET datasets uncover interaction between DHS in the mouse liver. (related to Fig. 6)
(A) Summary of the sequencing analysis for the three independent Pol II ChIA-PET experiments performed in this project. QC stands for quality check. **(B)** Number (black) and percentage

(blue) of Paired-End Tags (PET) based on the distance between the two reads for the three independent Pol II ChIA-PET experiments. Reads mapping to two different chromosomes are labeled as extra-chrom. reads. **(C)** Percentage of PET with non-chimeric half-linker barcodes (specific products, grey) and chimeric half-linker barcodes (non-specific products, black) for each of the three independent Pol II ChIA-PET experiments. **(D)** Distribution of the PET length for the non-chimeric PET (specific products, grey) and the chimeric PET (non-specific products, black), for the mouse liver Pol II ChIA-PET experiments performed with single crosslinked nuclei (left) or dual crosslinked nuclei (right). The ratio between non-chimeric PET and chimeric PET is overlaid in red. Both y-axes are represented in $\log_{10}$ scale. **(E)** Genome browser view of mouse liver BMAL1 ChIP-seq (this study), DNase-seq (ENCODE), and Pol II ChIP-seq (from Sobel et al. 2017). PETs with both reads mapped to DHSs are in red, while PETs with one read mapped to a DHS are in orange and those not mapped to a DHS are in grey.

Supplementary References

Boergesen M, Pedersen TA, Gross B, van Heeringen SJ, Hagenbeek D, Bindesboll C, Caron S, Lalloyer F, Steffensen KR, Nebb HI et al. 2012. Genome-wide profiling of liver X receptor, retinoid X receptor, and peroxisome proliferator-activated receptor alpha in mouse liver reveals extensive sharing of binding sites. *Molecular and cellular biology* **32**: 852-867.

Bunger MK, Wilsbacher LD, Moran SM, Clendenin C, Radcliffe LA, Hogenesch JB, Simon MC, Takahashi JS, Bradfield CA. 2000. Mop3 is an essential component of the master circadian pacemaker in mammals. *Cell* **103**: 1009-1017.

Cho H, Zhao X, Hatori M, Yu RT, Barish GD, Lam MT, Chong LW, DiTacchio L, Atkins AR, Glass CK et al. 2012. Regulation of circadian behaviour and metabolism by REV-ERB-alpha and REV-ERB-beta. *Nature* **485**: 123-127.

Consortium GT. 2013. The Genotype-Tissue Expression (GTEx) project. *Nature genetics* **45**: 580-585.

Croci O, De Fazio S, Biagioni F, Donato E, Caganova M, Curti L, Doni M, Sberna S, Aldeghi D, Biancotto C et al. 2017. Transcriptional integration of mitogenic and mechanical signals by Myc and YAP. *Genes & development* **31**: 2017-2022.

Dobin A, Davis CA, Schlesinger F, Drenkow J, Zaleski C, Jha S, Batut P, Chaisson M, Gingeras TR. 2013. STAR: ultrafast universal RNA-seq aligner. *Bioinformatics* **29**: 15-21.

Everett LJ, Le Lay J, Lukovac S, Bernstein D, Steger DJ, Lazar MA, Kaestner KH. 2013. Integrative genomic analysis of CREB defines a critical role for transcription factor networks in mediating the fed/fasted switch in liver. *BMC genomics* **14**: 337.

Faure AJ, Schmidt D, Watt S, Schwalie PC, Wilson MD, Xu H, Ramsay RG, Odom DT, Flicek P. 2012. Cohesin regulates tissue-specific expression by stabilizing highly occupied cis-regulatory modules. *Genome research* **22**: 2163-2175.

Fullwood MJ, Ruan Y. 2009. ChIP-based methods for the identification of long-range chromatin interactions. *Journal of cellular biochemistry* **107**: 30-39.

Gordon FK, Vallaster CS, Westerling T, Iyer LK, Brown M, Schnitzler GR. 2014. Research resource: Aorta- and liver-specific ERalpha-binding patterns and gene regulation by estrogen. *Mol Endocrinol* **28**: 1337-1351.

Heinz S, Benner C, Spann N, Bertolino E, Lin YC, Laslo P, Cheng JX, Murre C, Singh H, Glass CK. 2010. Simple combinations of lineage-determining transcription factors prime cis-regulatory elements required for macrophage and B cell identities. *Molecular cell* **38**: 576-589.

Hughes ME, Hogenesch JB, Kornacker K. 2010. JTK_CYCLE: an efficient nonparametric algorithm for detecting rhythmic components in genome-scale data sets. *Journal of biological rhythms* **25**: 372-380.

Koike N, Yoo SH, Huang HC, Kumar V, Lee C, Kim TK, Takahashi JS. 2012. Transcriptional architecture and chromatin landscape of the core circadian clock in mammals. *Science* **338**: 349-354.

Langmead B, Salzberg SL. 2012. Fast gapped-read alignment with Bowtie 2. *Nature methods* **9**: 357-359.

Leinonen R, Sugawara H, Shumway M, International Nucleotide Sequence Database C. 2011. The sequence read archive. *Nucleic acids research* **39**: D19-21.

Li G, Fullwood MJ, Xu H, Mulawadi FH, Velkov S, Vega V, Ariyaratne PN, Mohamed YB, Ooi HS, Tennakoon C et al. 2010. ChIA-PET tool for comprehensive chromatin interaction analysis with paired-end tag sequencing. *Genome biology* **11**: R22.

Lim HW, Uhlenhaut NH, Rauch A, Weiner J, Hubner S, Hubner N, Won KJ, Lazar MA, Tuckermann J, Steger DJ. 2015. Genomic redistribution of GR monomers and dimers

mediates transcriptional response to exogenous glucocorticoid in vivo. *Genome research* **25**: 836-844.
MacIsaac KD, Lo KA, Gordon W, Motola S, Mazor T, Fraenkel E. 2010. A quantitative model of transcriptional regulation reveals the influence of binding location on expression. *PLoS computational biology* **6**: e1000773.
Menet JS, Rodriguez J, Abruzzi KC, Rosbash M. 2012. Nascent-Seq reveals novel features of mouse circadian transcriptional regulation. *eLife* **1**: e00011.
Piper J, Assi SA, Cauchy P, Ladroue C, Cockerill PN, Bonifer C, Ott S. 2015. Wellington-bootstrap: differential DNase-seq footprinting identifies cell-type determining transcription factors. *BMC genomics* **16**: 1000.
Piper J, Elze MC, Cauchy P, Cockerill PN, Bonifer C, Ott S. 2013. Wellington: a novel method for the accurate identification of digital genomic footprints from DNase-seq data. *Nucleic acids research* **41**: e201.
Quinlan AR, Hall IM. 2010. BEDTools: a flexible suite of utilities for comparing genomic features. *Bioinformatics* **26**: 841-842.
Sobel JA, Krier I, Andersin T, Raghav S, Canella D, Gilardi F, Kalantzi AS, Rey G, Weger B, Gachon F et al. 2017. Transcriptional regulatory logic of the diurnal cycle in the mouse liver. *PLoS biology* **15**: e2001069.
Trapnell C, Roberts A, Goff L, Pertea G, Kim D, Kelley DR, Pimentel H, Salzberg SL, Rinn JL, Pachter L. 2012. Differential gene and transcript expression analysis of RNA-seq experiments with TopHat and Cufflinks. *Nature protocols* **7**: 562-578.
Yoshitane H, Ozaki H, Terajima H, Du NH, Suzuki Y, Fujimori T, Kosaka N, Shimba S, Sugano S, Takagi T et al. 2014. CLOCK-controlled polyphonic regulation of circadian rhythms through canonical and noncanonical E-boxes. *Molecular and cellular biology* **34**: 1776-1787.
Zhang J, Poh HM, Peh SQ, Sia YY, Li G, Mulawadi FH, Goh Y, Fullwood MJ, Sung WK, Ruan X et al. 2012a. ChIA-PET analysis of transcriptional chromatin interactions. *Methods* **58**: 289-299.
Zhang R, Lahens NF, Ballance HI, Hughes ME, Hogenesch JB. 2014. A circadian gene expression atlas in mammals: implications for biology and medicine. *Proceedings of the National Academy of Sciences of the United States of America* **111**: 16219-16224.
Zhang Y, Laz EV, Waxman DJ. 2012b. Dynamic, sex-differential STAT5 and BCL6 binding to sex-biased, growth hormone-regulated genes in adult mouse liver. *Molecular and cellular biology* **32**: 880-896.